Langmuir
Article
pubs.acs.org/Langmuir
© 2009 American Chemical Society

Double Stacking Faults in Convectively Assembled Crystals of Colloidal Spheres

Jan Hilhorst,[†] Vera V. Abramova,[‡] Alexander Sinitskii,[‡,¶] Nina A. Sapoletova,[‡] Kirill S. Napolskii,[‡] Andrey A. Eliseev,[‡] Dmytro V. Byelov,[†] Natali A. Grigoryeva,[§] Alexandra V. Vasilieva,[∥] Wim G. Bouwman,[⊥] Kristina Kvashnina,[#] Anatoly Snigirev,[▽] Sergey V. Grigoriev,[∥] and Andrei V. Petukhov[†,*]

[†]*Van 't Hoff Laboratory for Physical and Colloid Chemistry, Debye Institute for Nanomaterials Science, Utrecht University, Padualaan 8, 3584 CH Utrecht, The Netherlands,* [‡]*Department of Materials Science, M.V. Lomonosov Moscow State University, 119991 Moscow, Russia,* [§]*Faculty of Physics, Saint-Petersburg State University, 198504 Saint-Petersburg, Russia,* [∥]*Petersburg Nuclear Physics Institute, Gatchina, 188350 Saint-Petersburg, Russia,* [⊥]*Department RRR, Faculty of Applied Sciences, TU-Delft, 2629 JB Delft, The Netherlands,* [#]*DUBBLE Beamline BM26, ESRF, 6 rue Jules Horowitz, BP 220, F-38043 Grenoble Cedex 9, France, and* [▽]*ESRF, 6 rue Jules Horowitz, BP 220, F-38043 Grenoble Cedex 9, France.* [¶]*Present address: Department of Chemistry, Rice University, 6100 Main Street, Houston, Texas 77005*

Received March 20, 2009. Revised Manuscript Received April 15, 2009

Using microradian X-ray diffraction, we investigated the crystal structure of convectively assembled colloidal photonic crystals over macroscopic (0.5 mm) distances. Through adaptation of Wilson's theory for X-ray diffraction, we show that certain types of line defects that are often observed in scanning electron microscopy images of the surface of these crystals are actually planar defects at 70.5° angles with the substrate. The defects consist of two parallel hexagonal close-packed planes in otherwise face-centered cubic crystals. Our measurements indicate that these stacking faults cause at least 10% of stacking disorder, which has to be reduced to fabricate high-quality colloidal photonic crystals.

Downloaded by UNIV LIB UTRECHT on August 26, 2009 | http://pubs.acs.org
Publication Date (Web): May 4, 2009 | doi: 10.1021/la900983v

Introduction

Synthesis of high-quality colloidal crystals by convective assembly is a promising pathway toward the fast, cheap production of three-dimensional (3D) photonic crystals for application as novel functional materials.[1−4] In this process, a dispersion containing a low concentration of monodisperse colloids is slowly evaporated. This causes the colloids to self-assemble onto a substrate that is standing in the dispersion.

Because the crystal structure is of vital importance to the optical properties of the material, much effort has been spent on finding equilibrium crystal structures[5−9] and the mechanisms of crystal growth.[10−13] It is generally accepted that for convectively assembled crystals, the dominant structure resulting from experiments is face-centered cubic (fcc),[3,10,11] although the mechanism leading to this is still under investigation.[4,10,14]

Just as vital as the crystal structure is the presence of defects in a crystal. On the one hand, uncontrolled incorporation of defects can easily degrade the optical properties.[15−18] On the other hand, defect engineering allows one to gain control of light propagation.[19,20] Despite the importance of defects for crystal properties, few studies focus on the intrinsic disorder in colloidal crystals.[11,13,16]

We can distinguish several types of defects common to colloidal crystals. First of all, the crystals contain a high concentration of point defects. The absence of an attractive interparticle potential and the presence of polydispersity[21] cannot fully account for experimentally observed densities of vacancies and interstitials so that the kinetics of crystal growth should be involved.[11] Second, dislocations are also present in large quantities.[13,22] Because of the low stacking fault energy (on the order of 10^{-3} kT per particle[6] in the thermodynamic limit), these linear defects often split up in

*To whom correspondence should be addressed. E-mail: a.v.petukhov@uu.nl.

(1) Jiang, P.; Bertone, J. F.; Hwang, K. S.; Colvin, V. L. *Chem. Mater.* **1999**, *11*, 2132–2140.
(2) Blanco, A.; Chomski, E.; Grabtchak, S.; Ibisate, M.; John, S.; Leonard, S. W.; Lopez, C.; Meseguer, F.; Miguez, H.; Mondia, J. P.; Ozin, G. A.; Toader, O.; Van Driel, H. M. *Nature* **2000**, *405*, 437–440.
(3) Vlasov, Y. A.; Bo, X. Z.; Sturm, J. C.; Norris, D. J. *Nature* **2001**, *414*, 289–293.
(4) Norris, D. J.; Arlinghaus, E. G.; Meng, L.; Heiny, R.; Scriven, L. E. *Adv. Mater.* **2004**, *16*(16), 1393–1399.
(5) Bolhuis, P. G.; Frenkel, D.; Mau, S. C.; Huse, D. A. *Nature* **1997**, *388*, 235–236.
(6) Mau, S. C.; Huse, D. A. *Phys. Rev. E* **1999**, *59*(4), 4396–4401.
(7) Pusey, P. N.; Van Megen, W.; Bartlett, P.; Ackerson, B. J.; Rarity, J. G.; Underwood, S. M. *Phys. Rev. Lett.* **1989**, *63*(25), 2653–2656.
(8) Zhu, J.; Li, M.; Rogers, R.; Meyer, W.; Ottewill, R. H.; STS-73 Space Shuttle Crew; Russel, W. B.; Chaikin, P. M. *Nature* 1997, *387*, 883−885.
(9) Miguez, H.; Meseguer, F.; Lopez, C.; Mifsud, A.; Moya, J. S.; Vasquez, L. *Langmuir* **1997**, *13*, 6009–6011.
(10) Meng, L.; Wei, H.; Nagel, A.; Wiley, B. J.; Scriven, L. E.; Norris, D. J. *Nano Lett.* **2006**, *6*(10), 2249–2253.
(11) Wei, H.; Meng, L.; Jun, Y.; Norris, D. J. *Appl. Phys. Lett.* **2006**, *89*, 241913.
(12) Checoury, X.; Enoch, S.; Lopez, C.; Blanco, A. *Appl. Phys. Lett.* **2007**, *90*, 161131.
(13) Vekris, E.; Kitaev, V.; Perovic, D. D.; Aitchison, J. S.; Ozin, G. A. *Adv. Mater.* **2008**, *20*, 1110–1116.
(14) Brewer, D. D.; Allen, J.; Miller, M. R.; De Santos, J. M.; Kumar, S.; Norris, D. J.; Tsapatsis, M.; Scriven, L. E. *Langmuir* **2008**, *24*(23), 13683–13693.
(15) Li, Z. Y.; Zhang, Z. Q. *Phys. Rev. B* **2000**, *62*(3), 1516–1519.
(16) Rengarajan, R.; Mittleman, D.; Rich, C.; Colvin, V. *Phys. Rev. E* **2005**, *71*, 016615.
(17) Vlasov, Y. A.; Astratov, V. N.; Baryshev, A. V.; Kaplyanskii, A. A.; Karimov, O. Z.; Limonov, M. F. *Phys. Rev. E* **2000**, *61*(5), 5784–5793.
(18) Yannopapas, V.; Stefanou, N.; Modinos, A. *Phys. Rev. Lett.* **2001**, *86*(21), 4811–4814.
(19) Braun, P. V.; Rinne, S. A.; García-Santamaría, F. *Adv. Mater.* **2006**, *18*, 2665–2678.
(20) Rinne, S. A.; García-Santamaría, F.; Braun, P. V. *Nature Photonics* **2008**, *2*, 52–56.
(21) Pronk, S.; Frenkel, D. *J. Chem. Phys.* **2004**, *120*(14), 6764–6768.
(22) Meijer, J. M.; De Villeneuve, V. W. A.; Petukhov, A. V. *Langmuir* **2007**, *23*(7), 3554–3560.

Downloaded by UNIV LIB UTRECHT on August 26, 2009 | http://pubs.acs.org
Publication Date (Web): May 4, 2009 | doi: 10.1021/la900983v

Shockley partial dislocations accompanied by stacking faults, a third type of defect. Both the lattice distortions around a (partial) dislocation and the presence of stacking faults affect the optical properties of colloidal crystals.[16,18] It is therefore necessary to fully characterize these types of disorders to find ways to control them.

To date, the structure of convectively assembled crystals was mostly addressed using electron[9−13,23] or confocal optical[10,11] microscopy, which can be applied to rather limited sample volumes. The micro-optical spectroscopy technique[12,13,24] is able to unravel the stacking order over a macroscopically large sample but was only applied to thin crystals consisting of a few layers. Laser diffraction is often complicated by the too high refractive index contrast. Moreover, it can only be applied to the study of periodic structures with a sufficiently large periodicity,[25,26] as the laser wavelength has to be twice as small as the lattice periodicity to fulfill the Bragg condition in diffraction measurements.

To be able to characterize large crystalline areas and have access to a broad q-range, we choose X-ray diffraction with microradian resolution. Using this technique, we demonstrate the presence of a previously undefined type of defect found in convectively assembled crystals of polystyrene spheres. The diffraction data are supplemented by electron and atomic force microscopy (AFM).

Experimental Section

Colloidal crystals made of 425 nm polystyrene microspheres (relative standard deviation $< 5\%$) were grown by the convective assembly technique.[1−4,10−13] The spheres were synthesized by emulsifier-free emulsion polymerization of styrene using potassium persulphate as an initiator.[27] Glass microscope slides were immersed in an aqueous suspension of microspheres with a volume fraction of about 0.5%. The temperature of the film growth was 50 °C. The obtained sample thickness was about 15−20 layers.

The Ni photonic crystals with an inverse opal structure were fabricated by using similar colloidal crystals[28] as templates. These were assembled onto a thin conductive gold layer evaporated on a mica substrate. Convective assembly of colloids was followed by electrochemical deposition of nickel into the voids between the spheres in a three-electrode cell at room temperature. The counter electrode was a Pt wire, and the reference electrode was a saturated Ag/AgCl electrode connected to the cell via a Luggin capillary; a 0.1 M $NiCl_2$, 0.6 M $NiSO_4$, 0.3 M H_3BO_3, and 3.5 M C_2H_5OH solution was used for potentiostatic Ni deposition at a potential of $E_d = -0.9$ V vs the Ag/AgCl reference electrode. The polystyrene microspheres were subsequently dissolved in toluene.

Scanning electron micrographs of polystyrene and Ni photonic crystals were recorded on a LEO Supra VP 50 instrument. AFM images were recorded in tapping mode using a Digital Instruments Nanoscope IIIa atomic force microscope and Nanosensors Point Probe Plus NCH 50 silicon tips.

X-ray studies were performed at the Dutch-Belgian beamline BM-26 DUBBLE of the European synchrotron radiation facility (ESRF) in Grenoble, France. We used our recently developed microradian X-ray diffraction setup similar to the one described in refs 29 and 30. In brief, to achieve the maximum transverse coherence length of the beam, any focusing of the beam before the experimental hutch was avoided. Instead, the X-ray beam was focused by a set of compound refractive lenses (CRLs) at the phosphor screen of the CCD (charge-coupled device) X-ray detector (Photonic Science, 4008×2671 pixels of $22\ \mu m^2$) located at a distance of 8 m from the lens. The samples were placed just after the CRLs. Using computer-controlled motorized rotation and translation stages, the sample orientation (around two axes orthogonal to the beam) and its position (in two directions orthogonal to the beam) could be remotely changed. An X-ray photon energy of 13 keV (wavelength $\lambda = 0.095$ nm) was used. The beam diameter in the sample was 0.5 mm. This setup allows achievement of an angular resolution (full-width at half-maximum) of the order of 5 microradians, corresponding to 3.3×10^{-4} nm^{-1} in the reciprocal space.

Results and Discussion

Figure 1a−c presents examples of microradian diffraction patterns measured for different orientations of as-grown crystals of polystyrene spheres, corresponding to incidence of the X-ray beam along the [111], [110], and [001] crystallographic fcc directions, respectively, where the [111] direction runs perpendicular to the substrate. The corresponding views of a perfect fcc crystal in real space are shown in Figure 1d−f. The red spheres indicate the particles belonging to a single (111) plane parallel to the substrate.

In the diffraction patterns, one can clearly identify a large number of reflections, which can be assigned to the reciprocal lattice of the ideal fcc crystal structure (peak assignment and further details can be found in the Supporting Information). The 4-fold symmetry of the pattern in Figure 1c and the equal intensity of the four reflections of the 220 family suggest that a single fcc domain is illuminated. Visual inspection of the crystals revealed the vertical stripe pattern that is typical for convectively assembled crystals. These stripes originate from single fcc domains,[31,32] with a width of approximately the same size as the X-ray beam, confirming the possibility of obtaining diffraction data from a single domain.

In addition to the sharp Bragg peaks, one can also see two sets of extended Bragg rods in Figure 1b, which do not fit the ideal fcc crystal structure. These rods are parallel to the ⟨111⟩ crystallographic directions and indicate the presence of planar defects parallel to two types of close-packed hexagonal layers, which make an angle of 70.5° with the substrate. One of these close-packed {111} planes is highlighted in purple in Figure 1e.

The zero-order rods passing through the origin of the reciprocal space can be induced by distorted periodicity between the {111} planes, for example, by lattice distortions around a dislocation line. The visibility of the zero-order rods is greatly enhanced by a high form factor $F(q)$ (Figure 2a), indicating a small contribution from the structure factor. They are therefore not related to the strongest type of disorder in between the {111} planes. The form factor of the first- and the second-order Bragg rods is much smaller (Figure 2a), due to larger value of the scattering vector (Figure 2b). Their relatively high intensity therefore originates from a high structure factor, caused by

(23) Sinitskii, A. S.; Khokhlov, P. E.; Abramova, V. V.; Laptinskaya, T. V.; Tretyakov, Y. D. *Mendeleev Commun.* **2007**, *17*, 4–6.
(24) Schöpe, H. J.; Barreira Fontecha, A.; Konig, H.; Marques Hueso, J.; Biehl, R. *Langmuir* **2006**, *22*, 1828–1838.
(25) Amos, R. M.; Rarity, J. G.; Tapster, P. R.; Shepherd, T. J.; Kitson, S. C. *Phys. Rev. E* **2000**, *61*, 2929–2935.
(26) Sinitskii, A.; Abramova, V.; Laptinskaya, T.; Tretyakov, Y. D. *Phys. Lett. A* **2007**, *366*, 516–522.
(27) Goodwin, J. W.; Hearn, J.; Ho, C. C.; Ottewill, R. H. *Colloid Polym. Sci.* **1974**, *252*(6), 464–471.
(28) Napolskii, K. S.; Sinitskii, A.; Grigoriev, S. V.; Grigorieva, N. A.; Eckerlebe, H.; Eliseev, A. A.; Lukashin, A. V.; Tretyakov, Y. D. *Phys. B* **2007**, *397*, 23–26.
(29) Petukhov, A. V.; Thijssen, J. H. J.; 't Hart, D. C.; Imhof, A.; Van Blaaderen, A.; Dolbnya, I. P.; Snigirev, A.; Moussaid, A.; Snigireva, I. *J. Appl. Crystallogr.* **2006**, *39*, 137–144.
(30) Thijssen, J. H. J.; Petukhov, A. V.; 't Hart, D. C.; Imhof, A.; Van der Werf, C. H. M.; Schropp, R. E. I.; Van Blaaderen, A. *Adv. Mater.* **2006**, *18*, 1662–1666.
(31) Thijssen, J. H. J. Ph. D. Thesis, Chapter 5; Utrecht University, Utrecht, 2007; http://igitur-archive.library.uu.nl/dissertations/2007-0521-200321/index.htm.
(32) Andreani, L. C.; Balestreri, A.; Galisteo-López, J. F.; Galli, M.; Patrini, M.; Descrovi, E.; Chiodoni, A.; Giorgis, F.; Pallavidino, L.; Geobaldo, F. *Phys. Rev. B* **2008**, *78*, 205304.

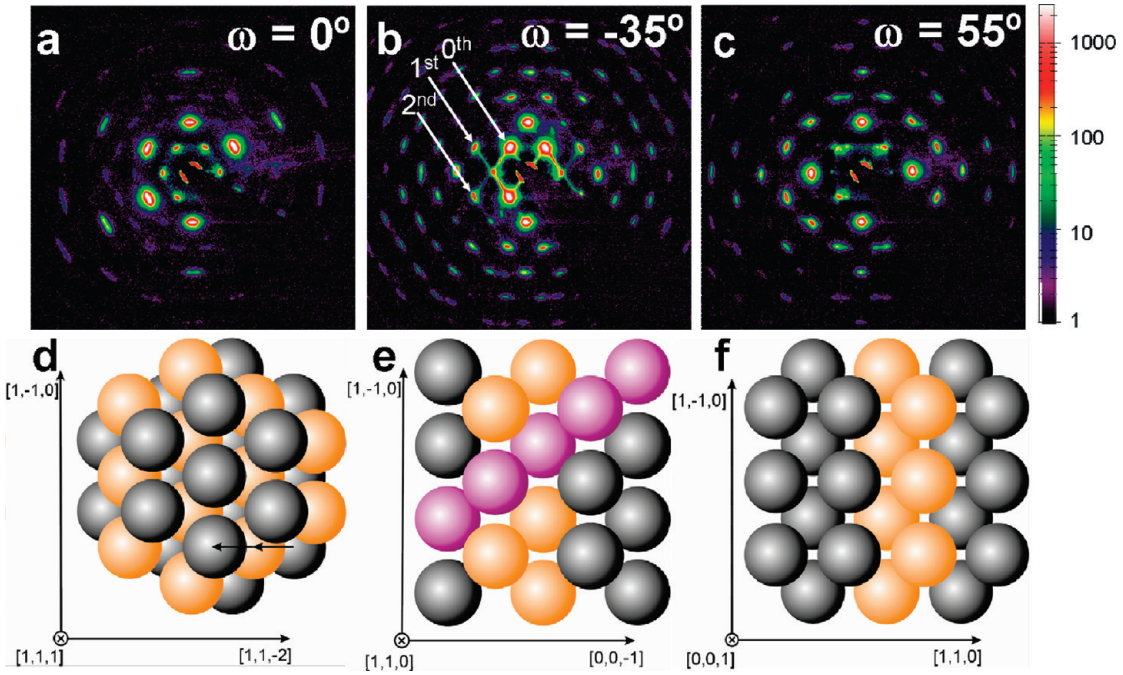

Figure 1. Microradian X-ray diffraction patterns measured with X-ray beam orthogonal to the substrate ($\omega = 0°$) and after a sample rotation around the vertical axis by $\omega = -35°$ and $\omega = 55°$ are shown in panels a−c. The arrows in panel b point to a set of Bragg rods of different order. A similar set of rods runs from the bottom left to the top right of the same image. The intensity scaling is explained in the scale bar next to panel c. Panels d−f represent real space fcc crystals with orientations corresponding to the diffraction images above them. Note that the real space structures correspond to perfect fcc lattices, while panels a−c represent measurements on real (faulted) crystals. The red spheres (color online) form a (111) plane parallel to the substrate in panels d−f. The purple spheres in panel e highlight a $(1\bar{1}1)$ plane.

stacking disorder in between the close-packed planes of colloidal spheres.[33,34]

From the intensity distribution along the first- and second-order Bragg rods, we can learn about the structure of the crystal under investigation. This intensity distribution is usually described by Wilson's theory,[35] which assumes that a crystal consists of an arbitrary sequence of close-packed layers in A, B, and C positions. The probability α of finding a close-packed layer in an fcc environment is independent of the stacking environment of the neighboring layers. Consequently, the probability of finding a close-packed layer in a hexagonal close-packed (hcp) environment is equal to $1 - \alpha$. The value of α uniquely determines the distribution of scattering intensity along a Bragg rod. Figure 2c shows the measured intensity profile along a first-order Bragg rod. It also shows a profile that was calculated within Wilson's theory for a crystal with dominant fcc stacking ($\alpha = 0.9$). One can see that the theory predicts two times as many maxima as observed experimentally. The reason for this discrepancy is related to the fact that in the Wilson model a single hcp layer changes the direction of the fcc growth from the ABC to ACB type stacking (Figure 2c, inset), giving rise to an additional set of Bragg reflections along the Bragg rod. Our data, however, suggest that only one growth direction dominates. This can only happen if the stacking disorder is caused by pairs of hcp layers. Such "double" stacking faults are in fact equivalent to sliding one part of a perfect fcc crystal relative to the other part along a {111} slip plane, creating two hcp layers bordering this plane (Figure 2d, inset).

To fit the data correctly, Wilson's theory was modified to account for double stacking faults only.[36] We assume that every subsequent layer is stacked in the positive x-direction (layers in Figure 1d are stacked in the negative x-direction, as indicated by the arrows) with a certain probability β. For high values of β (or analogously, $1 - \beta$), the majority of layers will be stacked in the positive (negative) x-direction, with only a small fraction of layers stacked the other way, creating the stacking faults. For an arbitrarily chosen pair of layers separated by m interlayer distances, there can be j steps in the negative x-direction and $m - j$ steps in the positive x-direction with the probability of $\{m!/[j!(m-j)!]\}(1-\beta)^j\beta^{m-j}$. For a first-order Bragg rod, the complex phases of their contributions to the structure factor will differ by $\Delta\varphi_m = 2\pi(m - 2j)/3 + 2\pi m(q_{\parallel}/q_{111})$, where $q_{\parallel}$ is the projection of the scattering vector onto the Bragg rod. A summation of the layer contributions averaged over all possible realizations (described in the Supporting Information in more detail) yields the statistically averaged structure factor profile along a first-order Bragg rod in the form

$$S_{10}(z) = \mathrm{Re}\left\{\frac{1+z}{1-z}\right\} \qquad (1)$$

where $z = \exp[2\pi i(q_{\parallel}/q_{111} - 1/3)][1 - \beta + \beta\exp(4\pi i/3)]$.

The intensity profile $I(q_{\parallel}) \propto S(q_{\parallel})\,F(q)$ along the first-order Bragg rod, calculated with the modified theory for $\beta = 0.9$ (Figure 2d), closely follows the experimental result. This fit confirms the predominant fcc stacking found by others,[4,10,12] albeit with a significant amount of stacking disorder in directions other than perpendicular to the substrate.

The presence of pairs of hcp layers in slanted hexagonal planes should lead to apparent line defects with a squarelike sphere arrangement in the hexagonal layers parallel to the substrate as illustrated in Figure 3. This exactly corresponds to the observation in Figure 4a, displaying an electron micrograph of the top surface of a colloidal crystal. One can clearly see the lines of squarelike particle arrangement that are typically observed at the

(33) Versmold, H. *Phys. Rev. Lett.* **1995**, *75*(4), 763–766.
(34) Petukhov, A. V.; Dolbnya, I. P.; Aarts, D. G. A. L.; Vroege, G. J.; Lekkerkerker, H. N. W. *Phys. Rev. Lett.* **2003**, *90*, 028304.
(35) Wilson, A. J. C. *Proc. R. Soc. London Ser. A* **1941**, *180*, 277–285.
(36) Paterson, M. S. *J. Appl. Phys.* **1952**, *23*(8), 805–811.

Downloaded by UNIV LIB UTRECHT on August 26, 2009 | http://pubs.acs.org
Publication Date (Web): May 4, 2009 | doi: 10.1021/la900983v

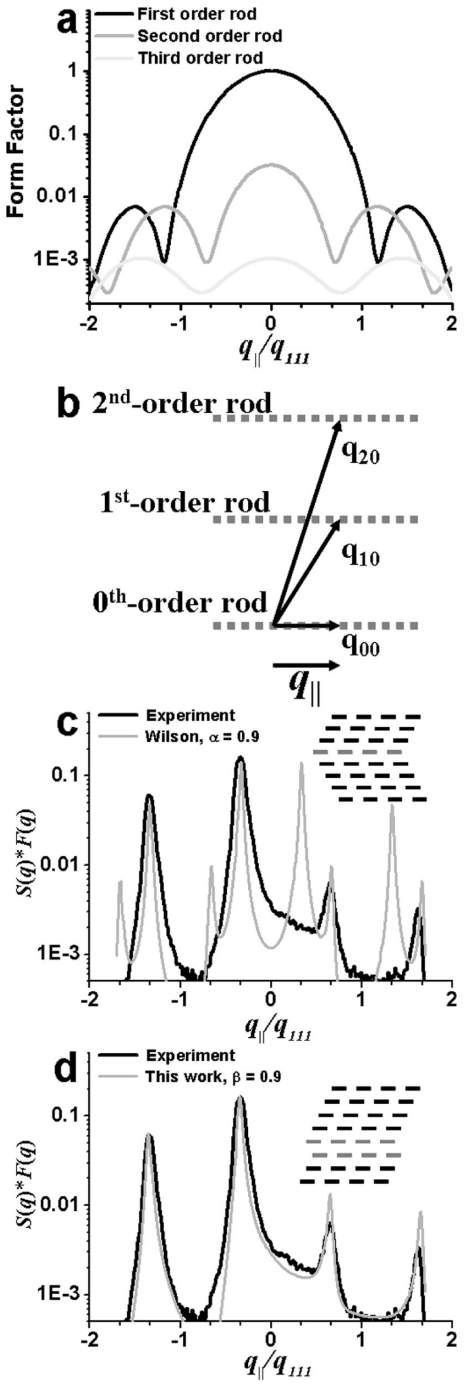

Figure 2. Panel a shows the variation of the form factor of 5% polydisperse spheres along the Bragg rods. The difference in the length of the wavevector for different Bragg rods is illustrated in (b). Panel c presents the profile of the scattering intensity along a first-order Bragg rod. The experimental result (black) is compared with a profile calculated within Wilson's theory (red). In panel d, the same result is compared to a profile calculated within the present model, which allows only for "double" stacking faults. The possible layer sequences in Wilson's theory and the present model are shown in the insets of panels c and d, respectively.

surface of convectively assembled colloidal crystals.[16,23] Our data suggest that these lines are in fact manifestations of planar defects.

In Figure 4b, we present a top view of a nickel-inverted crystal.[28] It is not surprising that the defects are also found here. Through the cavities, one can see a similar defect in the layer below the top layer, which confirms our conclusion that these line

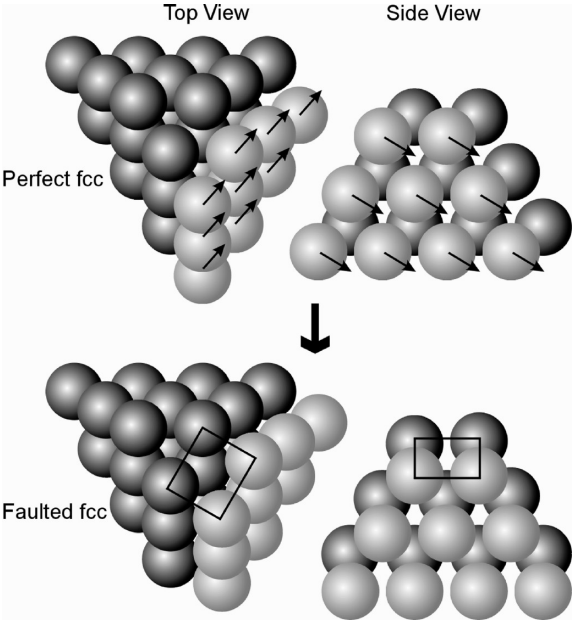

Figure 3. Top figures show a perfect fcc crystal, with the arrows indicating the direction of movement of the light gray {111} plane in the slip direction. The bottom figures illustrate the resulting structure. In the top view, the square packing of the particles can be observed. The side view shows the structure along the ⟨111⟩ direction perpendicular to the slip plane, illustrating that the resulting structure is still close-packed.

defects, at the surface of colloidal crystals, are in fact manifestations of double stacking faults. Their presence in inverted crystals is also evidenced by our X-ray results (not shown). The X-ray data obtained from the inverted crystal are similar to that presented in Figure 1. Similar sets of Bragg rods were observed at $\omega = \pm 35°$.

The slip vector for formation of the hcp planes not only moves the particles along the substrate to the positions of square coordination but also has a component perpendicular to the surface (Figure 3), leading to a height difference of one-third of the interplanar spacing in the ⟨111⟩ direction. This height difference was confirmed by AFM measurements (Figure 4c). The square configuration of the particles at a defect, as well as the height step, can be seen very clearly in this picture.

The fact that a height difference between two parts of a crystal is observed at their surface is not trivial. This difference must originate either at the substrate or somewhere in the crystal. Because height variations on a substrate are typically much smaller than the diameter of the colloids used for growing a crystal, it is unlikely that the stacking fault originates there; it would either generate a large void underneath the crystal or cause strong lattice distortions. Both are energetically unfavorable. The second option is that the faults originate inside the crystal. In this case, they would have to originate at a dislocation. A crystal starting out from a perfect fcc structure in the bottom layers could form a transition to a slanted fault via a Shockley partial dislocation. However, the first few layers of a convectively assembled crystal are predominantly hcp stacked[10,11] and contain a substantial concentration of Shockley partials influencing the stacking parallel to the substrate.[13] These Shockley partials could well be the nucleation point for the slanted faults, combining to a stair−rod dislocation, that is, two stacking faults on different {111} planes meeting on a single dislocation line. This is a structure that is regularly observed in crystals with low stacking fault energy, as the line energy of the dislocation is smaller than

Downloaded by UNIV LIB UTRECHT on August 26, 2009 | http://pubs.acs.org
Publication Date (Web): May 4, 2009 | doi: 10.1021/la900983v

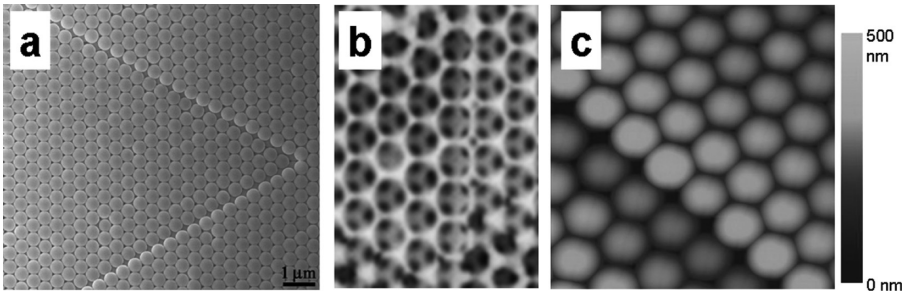

Figure 4. (a) Scanning electron microscopy (SEM) image of a colloidal crystal with the same orientation as during growth: The gravity direction runs from the top to the bottom of the figure. Two merging "line" defects can be observed, forming a locked stair-rod dislocation. (b) Zoom into the region of a slip defect in a SEM image of the surface of a Ni-inverted crystal. Notice the square arrangement of the air voids in the top layer and in the layer below with a lateral shift in between them. In an AFM image (c), the surface step at a defect is clearly visible. The vertical bar gives the height scale. The periodicity in panels b and c is the same as that of the colloidal crystal shown in panel a.

that of a single Shockley partial.[37] This hypothesis is currently under investigation.

In summary, we have investigated colloidal crystals grown by convective assembly through microradian X-ray diffraction, supported by scanning electron microscopy and AFM. We found that the cubic stacking order is accompanied by double stacking faults at an angle of 70.5° with the substrate, which manifest themselves as line defects on the crystal surface. The presence of up to 10% of stacking disorder in at least two out of four ⟨111⟩ directions may cause a significant degradation of the crystal properties, which was previously neglected in characterizations of the structure of convectively assembled crystals.

Acknowledgment. The Dutch Organisation for Scientific Research (NWO) is thanked for granting us beamtime at the DUBBLE beamline.

Supporting Information Available: Extensive peak assignment of the X-ray diffractograms in the main text and a mathematical derivation of the modification of Wilson's theory. This material is available free of charge via the Internet at http://pubs.acs.org.

(37) Hull, D.; Bacon, D. J. *Introduction to Dislocations*, 4th ed.; Elsevier Ltd.: Oxford, 2001.

Downloaded by UNIV LIB UTRECHT on August 26, 2009 | http://pubs.acs.org
Publication Date (Web): May 4, 2009 | doi: 10.1021/la900983v